

## RESEARCH ARTICLE

## The anisotropic scattering coefficient of sea ice

10.1002/2013JC009502

Christian Katlein<sup>1</sup>, Marcel Nicolaus<sup>1</sup>, and Chris Petrich<sup>2</sup>

## Key Points:

- Anisotropic scattering coefficients in sea ice influence radiance distribution
- Anisotropic distribution of under-ice radiance causes deeper light penetration
- Isotropic assumptions lead to significant errors in radiation models

## Correspondence to:

C. Katlein,  
Christian.Katlein@awi.de

## Citation:

Katlein, C., M. Nicolaus, and C. Petrich (2014), The anisotropic scattering coefficient of sea ice, *J. Geophys. Res. Oceans*, 119, doi:10.1002/2013JC009502.

Received 11 OCT 2013

Accepted 14 JAN 2014

Accepted article online 22 JAN 2014

<sup>1</sup>Alfred-Wegener-Institut Helmholtz-Zentrum für Polar- und Meeresforschung, Bremerhaven, Germany, <sup>2</sup>Norut Narvik AS, Narvik, Norway

**Abstract** Radiative transfer in sea ice is subject to anisotropic, multiple scattering. The impact of anisotropy on the light field under sea ice was found to be substantial and has been quantified. In this study, a large data set of irradiance and radiance measurements under sea ice has been acquired with a Remotely Operated Vehicle (ROV) in the central Arctic. Measurements are interpreted in the context of numerical radiative transfer calculations, laboratory experiments, and microstructure analysis. The ratio of synchronous measurements of transmitted irradiance to radiance shows a clear deviation from an isotropic under-ice light field. We find that the angular radiance distribution under sea ice is more downward directed than expected for an isotropic light field. This effect can be attributed to the anisotropic scattering coefficient within sea ice. Assuming an isotropic radiance distribution under sea ice leads to significant errors in light-field modeling and the interpretation of radiation measurements. Quantification of the light field geometry is crucial for correct conversion of radiance data acquired by Autonomous Underwater Vehicles (AUVs) and ROVs.

## 1. Introduction

The optical properties of sea ice are tightly linked to climate and biological productivity in polar oceans. Sea-ice albedo and light transmittance strongly impact the energy balance in the Arctic Ocean [Nicolaus *et al.*, 2012; Perovich *et al.*, 2011], and absorption of solar incoming energy affects surface and internal melting [Nicolaus *et al.*, 2010b; Zeebe *et al.*, 1996], leading to ice decay [Petrich *et al.*, 2012b]. Melt and decay of sea ice cause changes in its physical properties. Those properties like density, brine volume, and the internal structure of sea ice are determining its function as a habitat [Eicken *et al.*, 2002; Krembs *et al.*, 2011; Mundy *et al.*, 2005]. Good quantitative understanding of radiation partitioning is also important for assessment of the productivity of ice-borne microalgae [Ehn and Mundy, 2013; Ehn *et al.*, 2008a; Leu *et al.*, 2010].

Radiative transfer in sea ice has been widely studied using various numerical models and a large variety of measurements [e.g., Ehn *et al.*, 2008b; Light *et al.*, 2008; Mobley *et al.*, 1998; Pegau and Zaneveld, 2000; Trodahl *et al.*, 1987]. Nevertheless, knowledge about the optical properties of sea ice is still incomplete. While sea-ice albedo has been subject to considerable attention, knowledge about radiative transfer and absorption in sea ice is more limited due to the difficult access to the under-ice environment.

Due to the changes in properties of the Arctic sea ice such as younger ice age and decreased thickness [e.g., Haas *et al.*, 2008; Maslanik *et al.*, 2007; Perovich, 2011; Serreze *et al.*, 2007], the assumption of a homogeneous ice cover becomes increasingly invalid, in particular during summer when melt ponds develop [Nicolaus *et al.*, 2012; Roesel and Kaleschke, 2012] and the ice cover is transformed into a patchwork of various surface types. The larger heterogeneity of surface properties requires a better understanding of scattering properties and vertical radiation transfer, as recently highlighted in studies by Ehn *et al.* [2011] and Frey *et al.* [2011]. The discrepancy of models and observations [Frey *et al.*, 2011] also impacts estimates of the depth of the euphotic zone in ice-covered oceans [Bélanger *et al.*, 2013], which might be underestimated due to insufficient consideration of radiation partitioning in sea ice.

In sea ice, radiative transfer is subject to multiple scattering, altering the angular distribution of radiance [Petrich *et al.*, 2012a]. In order to obtain energy balance measurements, irradiance is typically measured on a horizontal planar interface. The downwelling planar irradiance  $F$  is defined as the integral of the radiance  $L$  incident from all angles of the upper hemisphere, weighed by the cosine of the zenith angle  $\theta$ ,

$$F = \int_{\phi=0}^{2\pi} \int_{\theta=0}^{\pi/2} L(\theta, \phi) \cos \theta \sin \theta d\theta d\phi, \quad (1)$$

where  $\theta$  and  $\phi$  is the azimuth angle.

Equation (1) describes the energy flux through a horizontal surface. Downwelling scalar irradiance  $F_{2\pi}$  is frequently used in biology, since the photosystems of autotrophic organisms are equally sensitive to photons from all incidence angles. It is defined analogously to equation (1),

$$F_{2\pi} = \int_{\phi=0}^{2\pi} \int_{\theta=0}^{\pi/2} L(\theta, \phi) \sin \theta d\theta d\phi. \quad (2)$$

As the azimuthal dependence of the radiance distribution is negligible under optically thick ice [Maffione et al., 1998; Pegau and Zaneveld, 2000], the radiance distribution in equation (1),  $L(\theta, \phi)$ , can be replaced by the zenith radiance  $L_0$  and the relative angular distribution of radiance  $f(\theta)$  with  $f(0^\circ) = 1$ ,

$$F = 2\pi \cdot L_0 \int_{\theta=0}^{\pi/2} f(\theta) \cos \theta \sin \theta d\theta. \quad (3)$$

When the radiance distribution under the sea ice is isotropic and thus  $f(\theta) = 1$ , equation (3) evaluates to  $F = \pi \cdot L_0$ . Although it is well known that even for strong scattering and in the asymptotic state of large optical thickness the radiance distribution of transmitted light does not become isotropic [Jaffé, 1960; Maffione et al., 1998; Pegau and Zaneveld, 2000; van de Hulst, 1980], an isotropic light field has been assumed frequently to convert between radiance and irradiance under sea ice [Frey et al., 2011; Grenfell, 1977; Roulet et al., 1974]. To provide a practical measure to convert between radiance and irradiance, we introduce the C value that depends on the angular distribution of radiance,  $f(\theta)$ :

$$C = \frac{F}{L_0}. \quad (4)$$

C is the ratio of irradiance  $F$  to zenith radiance  $L_0$ . Combining equations (3) and (4), the C value can also be obtained from a direct measurement of the radiance distribution  $f(\theta)$  under sea ice,

$$C = 2\pi \int_{\theta=0}^{\pi/2} f(\theta) \cos \theta \sin \theta d\theta. \quad (5)$$

Equations (1)–(5) describe the geometry of the light field and are valid for both monochromatic light and wavelength integrated broadband fluxes.

While most studies of inherent optical properties of sea ice treated sea ice as optically isotropic [e.g., Ehn et al., 2008b; Light et al., 2003; Maffione et al., 1998; Mobley et al., 1998], Trodahl et al. [1987] introduced the idea of an anisotropic scattering coefficient to explain their measurements. The only measurements of the radiance distribution of transmitted light under sea ice appear to be those of Trodahl et al. [1989]. However, the radiance distribution has been studied within sea ice [Pegau and Zaneveld, 2000] and for a laser beam leaving the upper surface of the sea ice [Schoonmaker et al., 1989]. Trodahl et al. [1987] found that light transfer could be described by assuming a scattering coefficient that is greater horizontally than vertically, which manifests itself in a greater extinction of “laterally propagating light” [Zhao et al., 2010]. The stronger extinction of light traveling horizontally changes the radiance distribution in such a way that the resulting light field is more downward directed [Trodahl et al., 1987] (Figure 1).

As nomenclature of anisotropy in scattering can be ambiguous, we want to clarify the nomenclature used in the following. In most of the literature, “anisotropic scattering” refers to the anisotropy of the scattering

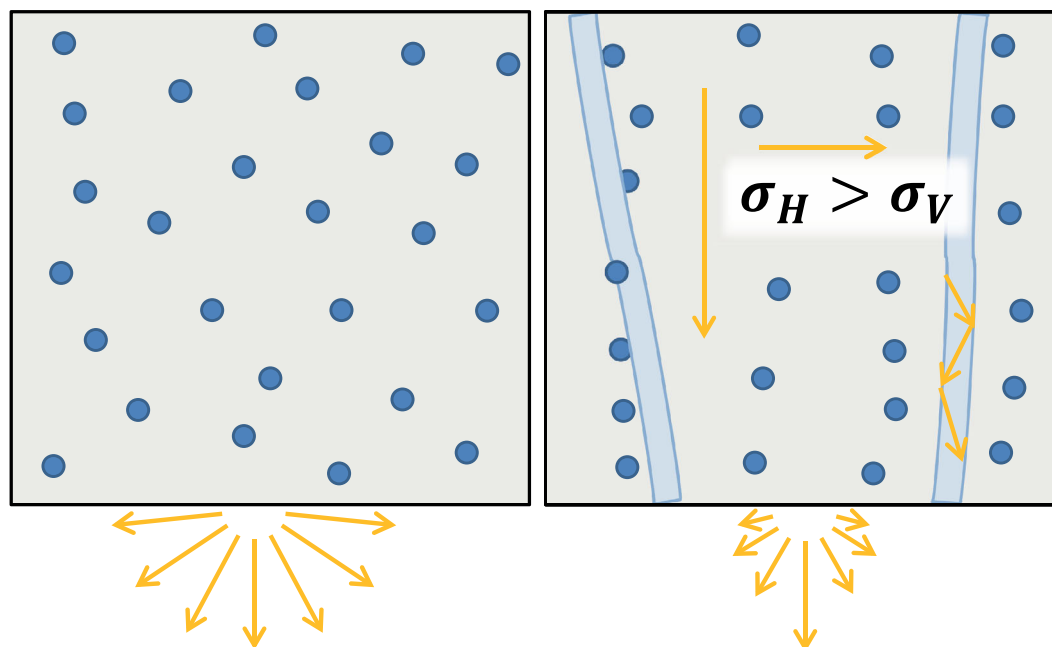


**Figure 1.** (left) In standard radiative transfer models scatterers (blue circles) are distributed randomly and homogenous throughout the medium. (right) Scatterers in sea ice are predominantly aligned along the lamellar crystal structure causing the anisotropy of the scattering coefficient. Anisotropic light extinction changes the shape of the radiance distribution underneath the sea ice.

phase function. Here we examine the effects of the anisotropic optical properties of the scattering medium on the radiance distribution exiting the sea ice. In this paper, we use the term anisotropy always to indicate that the effective scattering coefficient is dependent on the direction of light travel.

The objective of this paper is to investigate the angular radiance distribution below sea ice and its impact on the under-ice light-field and radiation measurements.

## 2. Methods

### 2.1. ROV Measurements

All measurements were performed during the expedition ARK-XXVII/3 (IceArc 2012) of the German research icebreaker *Polarstern* to the central Arctic from 2 August to 8 October 2012. We conducted synchronous measurements of spectral downwelling irradiance and radiance under sea ice using RAMSES-ACC (irradiance) and RAMSES-ARC (radiance) spectral radiometers (TriOS GmbH, Rastede, Germany) carried onboard a V8Sii Remotely Operated Vehicle (ROV) (Ocean Modules, Åtvidaberg, Sweden). ROV Observations were conducted within 1–2 m from the ice underside, yielding sensor footprint diameters of around 3.0 and 0.15 m for irradiance and radiance, respectively [Nicolaus *et al.*, 2010a]. Using synchronous measurements of downwelling irradiance at the surface, we obtained a large data set of 14,700 pairs of sea-ice transmittance and transreflectance. Transreflectance was introduced by Nicolaus and Katlein [2013] as the ratio of transmitted zenith radiance to downwelling irradiance at the surface, while transmittance is defined as the ratio of transmitted downwelling irradiance to downwelling irradiance at the surface. In addition to the setup previously described by Nicolaus and Katlein [2013], the ROV was equipped with an ultra-short-baseline (USBL) positioning system. The ROV attitude was recorded to give precise inclination information for the optical sensors and thus the possibility to measure the angular radiance distribution directly by rolling the ROV to the side underneath homogenous sea ice.

### 2.2. Lab Experiments

To measure the anisotropic nature of light extinction in the laboratory at  $-20^{\circ}\text{C}$ , we used a setup similar to the one of Grenfell and Hedrick [1983]. Sea-ice samples were obtained from the bottommost part of a 12 cm-diameter ice core. As the anisotropy of the scattering coefficient is a feature of multiple scattering,

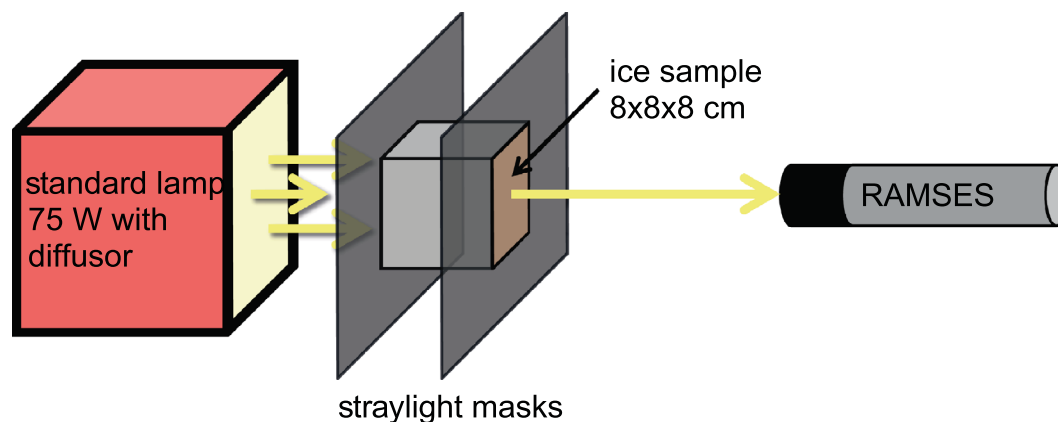


**Figure 2.** Sketch of the experimental setup to measure horizontal and vertical light extinction.

the sample size was chosen considerably bigger than in previous studies [Grenfell and Hedrick, 1983; Miller *et al.*, 1997]. Cubic samples with an edge length of  $8 \pm 0.1$  cm were cut from the core using a band saw. All surfaces were brushed clean from ice cuttings, smoothed with sandpaper, and finally polished with bare hands to obtain a clear surface. Exact sample sizes were measured with a caliper and samples were weighed onboard the ship to determine porosity using equations from Cox and Weeks [1983]. Between preparation and measurements, samples were packed in plastic wrapping to avoid further sublimation.

As shown in Figure 2, the samples were placed on a black stage and illuminated through a diffuser plate (ground glass) with a standard 75 W light bulb (OSRAM, München, Germany). The light bulb provided a stable diffuse light source over the measured wavelength range (320–950 nm) and the duration of the experiments. The lamp output was measured to be stable within  $\pm 1\%$ . Cardboard masks with a  $7 \times 7$  cm<sup>2</sup> rectangular opening were placed at both sides of the samples to avoid stray light entering the detector and to reduce the influence of imperfect sample edges. The light exiting the sample was registered by a RAMSES-ARC sensor measuring spectral radiance with a field of view of approximately  $7^\circ$ . The sensor was mounted at a distance of either 17.5 cm or 32.7 cm from the sample to register light emerging from a circular area with a diameter of  $\sim 2$  cm and 4 cm, respectively.

The transmitted normal radiance was measured for all six possible sample orientations. To reduce the influence of sample inhomogeneity, measurements from opposite sample orientations were averaged. As no anisotropy was observed in the horizontal plane, we averaged all four measurements of horizontal extinction. Radiance extinction coefficients  $\kappa_L$  were computed from

$$\kappa_L = \frac{-\ln \frac{L_{\text{sample}}}{L_{\text{empty}}}}{l}, \quad (6)$$

with radiance measured with and without sample in the sample holder  $L_{\text{sample}}$  and  $L_{\text{empty}}$ , respectively, and sample size,  $l$ .

Horizontal and vertical thin sections were prepared from ice cuttings left over from preparation of the cubic samples. They were photographed between crossed polarizers with a digital camera. Ice crystal and pore geometries were subsequently analyzed using the image processing software *JMicroVision*.

### 2.3. Radiative Transfer Model

As anisotropic inherent optical properties are currently not resolved in most radiative transfer models [e.g., Hamre *et al.*, 2004; Kokhanovsky and Zege, 2004], we used a Monte Carlo ray tracing model to evaluate the effect of the anisotropic scattering coefficient in sea ice. The Monte Carlo model was described in detail by Petrich *et al.* [2012a]. It is a three-dimensional, single-layer model designed to simulate anisotropic scattering coefficients as defined by Trodahl *et al.* [1987]. In the model, photons are tracked through a homogenous slab of a scattering medium. Directions of photon travel are changed by scattering events. The frequency of scattering events is determined from the scattering coefficient that in our anisotropic case is dependent on the

photon travel direction. The instantaneous scattering coefficient for a photon traveling at angle  $\theta$  is calculated during the runtime of the model as  $\sigma = \sigma_v + (\sigma_h - \sigma_v) \sin \theta$  [Petrich *et al.*, 2012a; Trodahl *et al.*, 1987]. We used the model to evaluate the effect of the anisotropic scattering coefficient on radiative transfer in a typical slab of sea ice. The ice thickness in the simulations was 1 m. This is a typical thickness of arctic first year ice [Haas *et al.*, 2008] and thick enough to ensure that the asymptotic state of the light field has been reached in unponded sea ice [Pegau and Zaneveld, 2000], resulting in an emerging light-field independent of the light-field incident on the surface. Common values for the asymmetry parameter of the phase function,  $g = 0.98$ , and the effective (isotropic) scattering coefficient  $\sigma_{eff} = \sigma(1-g) = 2 \text{ m}^{-1}$  were chosen according to the available literature [Haines *et al.*, 1997; Light *et al.*, 2008; Mobley *et al.*, 1998; Pegau and Zaneveld, 2000; Perovich, 1990; Petrich *et al.*, 2012a]. The anisotropy of the scattering coefficient is described similar to Trodahl *et al.* [1989] by the relation of vertical and horizontal scattering coefficients  $\sigma_v$  and  $\sigma_h$ , respectively, as

$$\gamma = 1 - \frac{\sigma_v}{\sigma_h} \tag{7}$$

and was varied between  $\gamma = 0$  and  $\gamma = 0.8$  guided by the values presented by Haines *et al.* [1997]. The horizontal scattering coefficient,  $\sigma_h$ , is always greater than  $\sigma_v$  for sea ice. Transmittance depends nontrivially on both  $\sigma_h$  and  $\sigma_v$ . To keep the transmittance constant while varying anisotropy values  $\gamma$ , both scattering coefficients need to be adjusted simultaneously. We used an empirical scaling law to estimate the vertical and horizontal scattering coefficients from  $\sigma_{eff}$  and  $\gamma$  in the absence of absorption,

$$\begin{aligned} \sigma_v &= \sigma_{eff} (1-\gamma)^{0.78} \\ \sigma_h &= \sigma_{eff} (1-\gamma)^{-0.22} \end{aligned} \tag{8}$$

Using equation (8), the bulk transmittance remained constant to within  $\pm 1\%$  of the transmittance value for the scattering coefficients and anisotropies used in this study. We performed 40 simulations with different anisotropy and scattering coefficients, each with  $10^6$  photons. As our goal was to explore the effect of anisotropic scattering on the radiance distribution, simulations were performed without absorption.

#### 2.4. Geometric Light-Field Model

To assess the influence of an anisotropic radiance distribution and ice covers with spatially varying surface properties such as ponded sea ice on light availability and under-ice radiation measurements, we used a two-dimensional geometric light-field model similar to the one presented by Frey *et al.* [2011]. Planar and scalar irradiances normalized to incident fluxes were calculated for points at depth  $z$  and horizontal position  $x$  along a discretized surface. Depth  $z$  is the distance to the underside of the ice. While absorption in the water column is taken into account by an exponential decay law, scattering in the water column is neglected. This is an appropriate assumption for clear Arctic waters. Planar downwelling irradiance at each point is then defined as the sum over all contributing discrete angles  $\theta$  covering a solid angle interval of  $\delta\Omega$ ,

$$F_D(x, z) = \frac{2}{\pi} \sum_{\theta=-90^\circ}^{90^\circ} L(\theta, \gamma) \cdot \exp(-\kappa_{abs} \cdot d(\theta, z)) \cdot \cos \theta \cdot \delta\Omega, \tag{9}$$

with distance of the grid point to the respective surface point,  $d$ , absorption coefficient of seawater,  $\kappa_{abs}$ , and radiance reaching the grid cell from the respective surface point,  $L(\theta)$ . Seawater absorption was set to  $\kappa_{abs} = 0.1 \text{ m}^{-1}$  as an average of observed broadband absorption coefficients obtained from depth profiles measured with the ROV during the campaigns. The angular dependence of the radiance exiting the ice  $L(\theta)$  is derived from the Monte Carlo Simulations and is dependent on the anisotropy of the scattering coefficient  $\gamma$ .  $L(\theta)$  was obtained by scaling the modeled  $f(\theta)$  in such a way, that the planar irradiance directly under a homogenous sea-ice cover is independent of  $\gamma$ .

To evaluate the effect of the anisotropic scattering coefficient of sea ice on the under-ice light field, we simulated one real surface profile from station PS80/224 and various artificial surface geometries with different melt-pond concentrations and melt-pond sizes. Following Nicolaus *et al.* [2012], the transmittance of ponded and bare ice was set to 0.22 and 0.04, respectively.

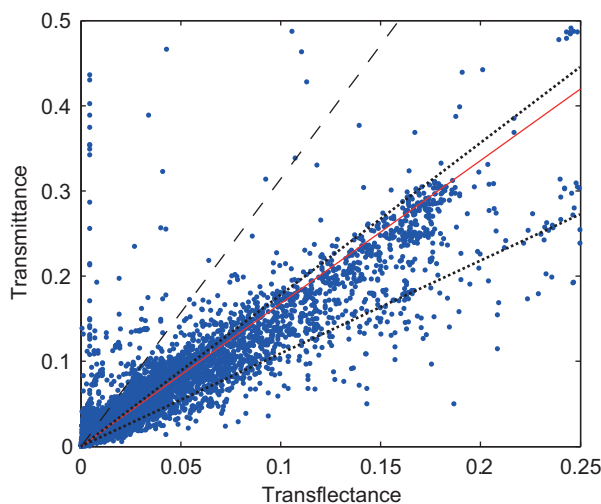


**Figure 3.** Transmittance  $T_F$  versus transflectance  $L_0$ , for all ROV measurements conducted during IceArc 2012 (blue dots). The dashed black and red lines follow  $F = C \cdot L_0$  with  $C = \pi$  and  $C = 1.68$ , respectively. Dotted lines give the range for measured values of  $C$  (upper line:  $C = 1.76$ ; lower line:  $C = 1.09$ ).

### 3. Results

Measurements of the light field beneath Arctic sea ice resulted in values of  $C$  significantly different from  $\pi$ . The plot of measured transmittance versus transflectance (Figure 3) shows that  $C$  values ranged from 1.09 to 1.76 with a median of all measurements of  $C = 1.68$  (Table 1). The ratio of transmittance  $T_F$  and transflectance  $T_L$  represents an observationally robust way to determine the  $C$  value. No direct dependence of single  $C$  value measurements and the distance to the ice or ice thickness was found.  $C$  values were only weakly dependent on wavelength for most of transmitted light between 400 and 600 nm where

scattering dominates over absorption. Thus,  $C$  values between 400 and 600 nm are similar to those obtained from wavelength integrated broadband measurements. At wavelengths below 400 nm and larger than 600 nm, where absorption becomes more important [Grenfell and Perovich, 1981],  $C$  values decrease. The magnitude of this decrease varies with the strength of absorption. This independence of wavelength between 400 and 600 nm supports the hypothesis that the light field underneath sea ice is strongly influenced by the anisotropy of the scattering coefficient, as scattering in sea ice is known to be approximately independent of wavelength [Grenfell and Hedrick, 1983].

Results from the laboratory experiments are presented in Table 2. A clear difference of light extinction was observed between horizontal and vertical sample orientations. The extinction coefficient in the horizontal direction was up to 37% greater than in the vertical direction. Only sample 5 showed different extinction characteristics, which can be readily explained by the inhomogeneity of a thin strongly scattering layer combined with rather transparent ice.

The anisotropy of the scattering coefficient was also evident from direct measurements of the radiance distribution, obtained by rolling the ROV underneath the sea ice. The measured shape of the radiance distribution could be reproduced by model results assuming an anisotropic scattering coefficient (Figure 4).

While results for  $\gamma = 0$  reproduced results from diffusion theory [Kokhanovsky and Zege, 2004] and the Eddington approximation [van de Hulst, 1980], the radiance distribution becomes increasingly downward

**Table 1.** Overview of Median  $C$  Values, Their Standard Deviation, and Derived  $\gamma$  Values Observed From ROV-Based Synchronous Measurements of Downwelling Irradiance and Radiance<sup>a</sup>

| Station Number | Date        | $\bar{C}$ | STD   | $\rightarrow \gamma$ | $z_{ice}$ | Sea Ice/Clouds                                              |
|----------------|-------------|-----------|-------|----------------------|-----------|-------------------------------------------------------------|
| PS80/224       | 10 Aug 2012 | 1.73      | 0.72  | 0.38                 | 1.0–1.5   | FYI, partly cloudy, melting                                 |
| PS80/237       | 15 Aug 2012 | 1.76      | 2.16  | 0.37                 | 1.2–2.0   | FYI, overcast, melting                                      |
| PS80/255       | 20 Aug 2012 | 1.70      | 1.90  | 0.40                 | 0.7–1.2   | FYI, overcast                                               |
| PS80/323       | 4 Sep 2012  | 1.65      | 16.62 | 0.43                 | 1.2–1.7   | FYI, overcast                                               |
| PS80/335       | 8 Sep 2012  | 1.68      | 6.71  | 0.41                 | 0.9–1.7   | FYI, overcast, roll experiment                              |
| PS80/349       | 18 Sep 2012 | 1.63      | 3.50  | 0.43                 | 1.2–1.8   | MYI, overcast                                               |
| PS80/360       | 22 Sep 2012 | 1.09      | 13.32 | 0.71                 | 1.1–1.8   | FYI, overcast, roll experiment, high abundance of ice algae |
| PS80/384       | 29 Sep 2012 | 1.76      | 4.66  | 0.37                 | 1.0–1.4   | FYI, overcast, revisited floe of PS80/224                   |
| Median         | 2012        | 1.68      | 9.02  | 0.41                 |           |                                                             |

<sup>a</sup>Station numbers are official Polarstern station numbers. For all stations the main ice type, as well as information on cloud cover is given.



**Table 2.** Physical Properties of Samples From Laboratory Experiments<sup>a</sup>

| Sample Number  | Station  | Date        | Density (g/cm <sup>3</sup> ) | Porosity (%) | $\kappa_H/\kappa_V$ | C    | Crystal Elongation |
|----------------|----------|-------------|------------------------------|--------------|---------------------|------|--------------------|
| 1              | PS80/255 | 21 Aug 2012 | 0.81                         | 12.5         | 1.26                | 2.09 | 5.06               |
| 2              | PS80/224 | 10 Aug 2012 | 0.75                         | 18.5         | 1.38                | 1.95 | 4.89               |
| 3              | PS80/323 | 5 Sep 2012  | 0.83                         | 9.4          | 1.16                | 2.22 | 3.73               |
| 4              | PS80/335 | 8 Sep 2012  | 0.89                         | 3.4          | 1.07                | 2.37 | 4.36               |
| 5 <sup>b</sup> | PS80/349 | 19 Sep 2012 | 0.85                         | 7.5          | 0.95                | 2.37 | 6.74               |
| 6              | PS80/360 | 22 Sep 2012 | 0.78                         | 15.4         | 1.33                | 2.00 | 4.10               |
| 7              | PS80/384 | 29 Sep 2012 | 0.90                         | 2.6          | 1.10                | 2.32 | 3.70               |

<sup>a</sup>Porosity was calculated from the measured density, C values are derived from the quotient of measured extinction coefficients in the horizontal and vertical direction  $\kappa_H/\kappa_V$ . Crystal elongation gives the length to width ratio of the columnar ice crystals determined from thin section analysis.

<sup>b</sup>Vertically inhomogeneous sample.

peaked for growing  $\gamma$ . To obtain an empirical equation for the radiance distribution as a function of  $\gamma$ , the modeled radiance distributions were fitted with a two-dimensional surface using the MATLAB Curve-Fitting toolbox ( $R^2 = 0.991$ ), resulting in

$$f^*(\theta, \gamma) = \left( \frac{1}{3} + \frac{2}{3} \cos \theta \right) \cos \theta (1 - \gamma) + \gamma \exp((-0.05681 \pm 0.00072)\theta) \quad (10)$$

with  $f(\theta) = f^*/\cos \theta$ . This equation allows for the calculation of the radiance distribution under an optically thick ice cover for broadband quantities or between 400 and 600 nm when extinction is dominated by scattering. To obtain C values, the modeled radiance distributions were integrated numerically and the results

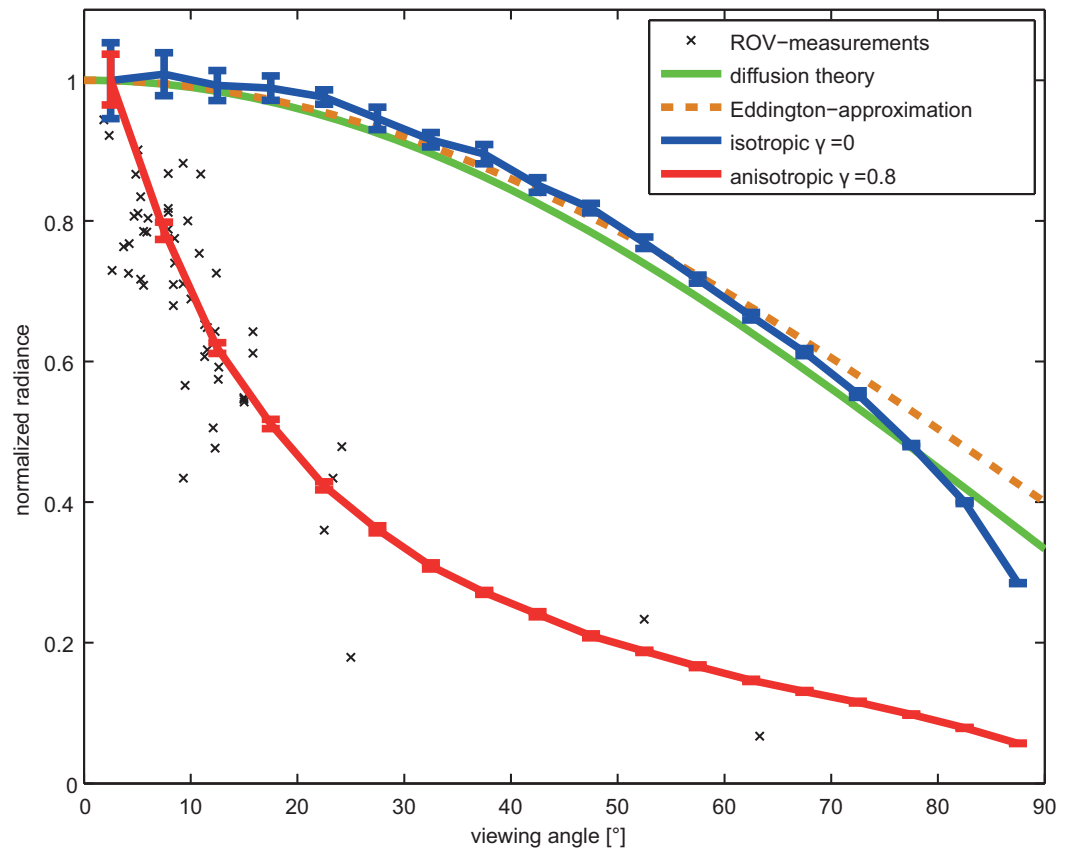


**Figure 4.** Angular distribution of radiance leaving the underside of sea ice. Results of the Monte Carlo model for the isotropic scattering coefficient  $\gamma = 0$  (blue line) compare well with the approximation from diffusion theory (green line) and the Eddington approximation (dashed orange line). Measurements from the ROV-roll experiment on station PS80/335 on 8 Sep 2012 (crosses) are shown together with results of the model with anisotropic scattering coefficient  $\gamma = 0.8$  (red line). Error bars indicate the azimuthal standard deviation of modeled photon counts.

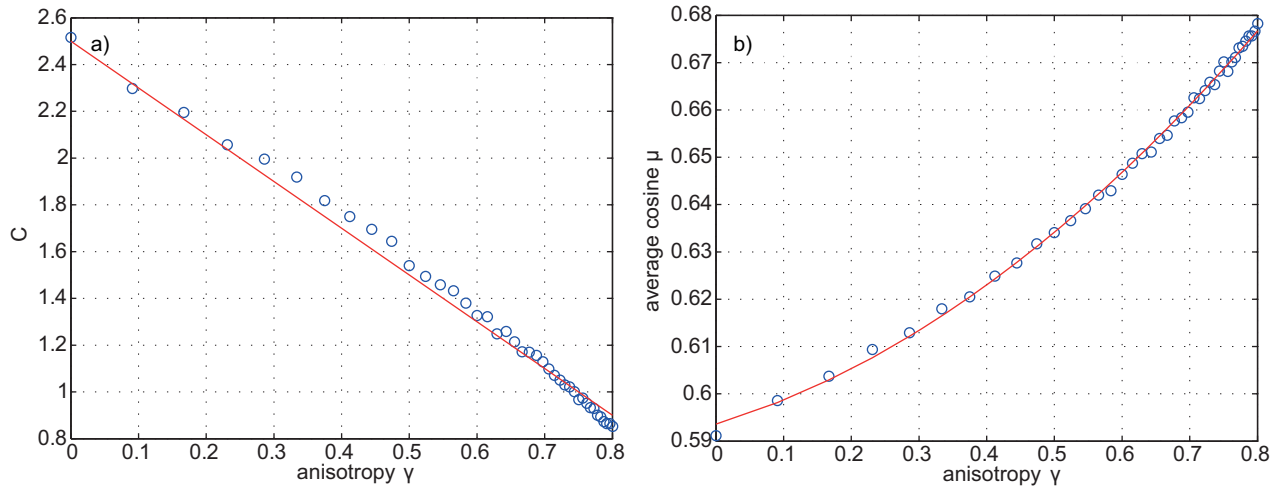


**Figure 5.** (a) The ratio of irradiance and radiance ( $C$  value) observed underneath the sea ice as a function of the anisotropy of the scattering coefficient  $\gamma$ . Blue circles show the results of Monte Carlo simulations, while the red line depicts the suggested parameterization  $C = 2.5 - 2\gamma$ . (b) Average cosine underneath the sea ice as a function of anisotropy  $\gamma$ .

plotted against  $\gamma$  (Figure 5). Surprisingly,  $C$  values could be described by a simple linear expression ( $R^2 = 0.990$ ),

$$C = 2.5 - 2\gamma. \tag{11}$$

Equation (11) can be used to determine the  $C$  value of a radiance distribution emitted from an optically thick ice cover with the known anisotropy of the scattering coefficient  $\gamma$ . This parameterization shows that the  $C$  value does not reach  $\pi$  even for isotropic scattering. In fact,  $C = 2.5$  for isotropic media is in agreement with the theoretical  $C$  values derived from both photon diffusion theory [Kokhanovsky and Zege, 2004] and the Eddington approximation [van de Hulst, 1980] of 2.49 and 2.51, respectively.

The consequences of an anisotropic radiance distribution exiting the sea ice for the under-ice light field were explored with the two-dimensional geometric light-field model. Figure 6 shows the irradiance field calculated for a 450 m long profile of pond cover obtained from an aerial picture of the ice station PS80/224 on 9 August 2012. The relative differences in downwelling irradiance between  $\gamma = 0$  and  $\gamma = 0.6$  are in the range of 10% and would thus be accessible to measurements as measurement uncertainties are smaller

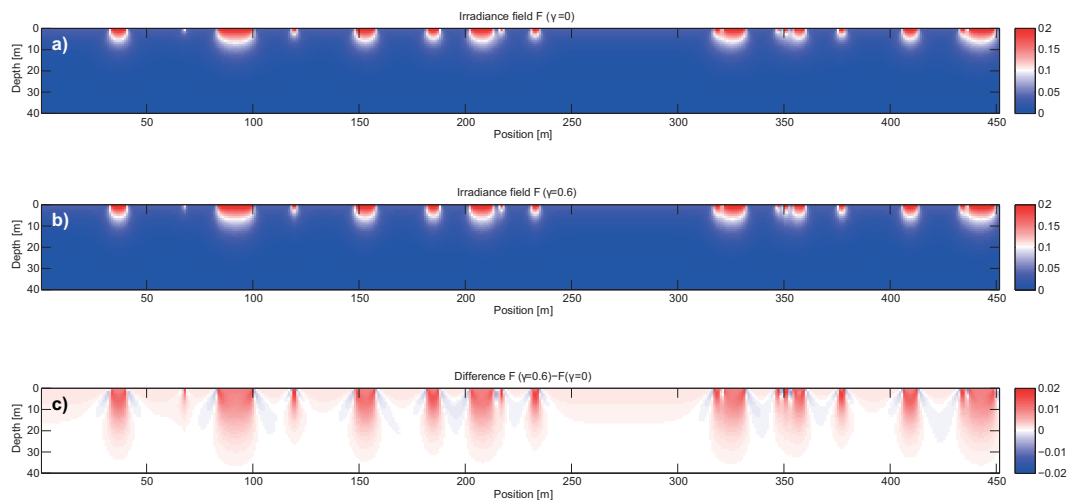


**Figure 6.** (a) Irradiance field calculated for a 450 m long horizontal profile of pond coverage taken from an aerial picture of ice station PS80/224. Transmittances for ponds and bare ice were 0.22 and 0.04, respectively. (b) Same irradiance field but calculated for anisotropic scattering coefficient in sea ice with  $\gamma = 0.6$ . (c) Difference between the irradiance fields resulting from anisotropic and isotropic scattering coefficient of the sea ice.



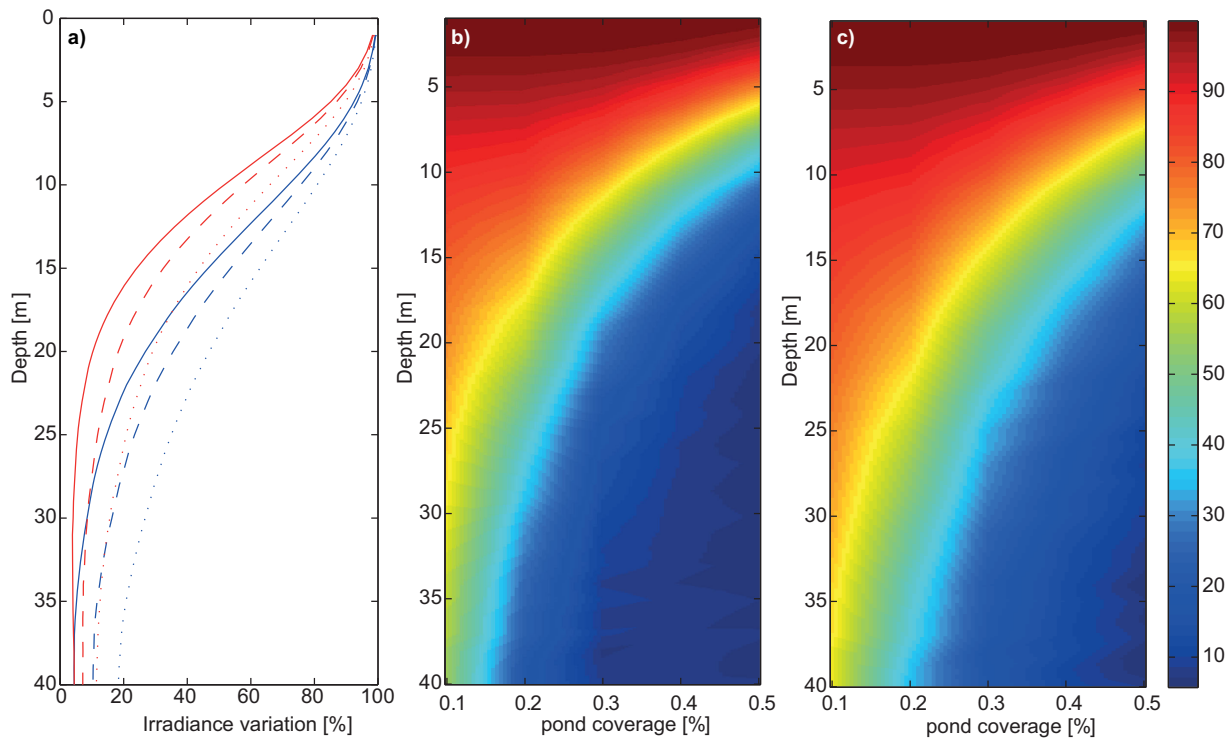


**Figure 7.** (a) Depth-dependent irradiance variation  $\beta$  for different anisotropies ( $\gamma = 0$  solid line,  $\gamma = 0.3$  dashed line,  $\gamma = 0.6$  dotted line), a regular ice cover with pond coverages of 30% (blue) and 40% (red) and a pond size of 7.5 m. Irradiance variation at depth in dependence of pond coverage for a pond size of 7.5 m, (b)  $\gamma = 0$  and (c)  $\gamma = 0.6$ , respectively.

[Nicolaus and Katlein, 2013; Nicolaus et al., 2010a]. Irradiance levels under melt ponds are generally higher for large  $\gamma$ . This effect is especially pronounced close to the surface up to a depth of approximately 10 m, where the differences are greatest.

Under-ice measurements of radiation under heterogeneous sea-ice covers are highly dependent on the distance between sensors and the ice underside. While radiance sensors provide good spatial resolution even when operated at depth, the ability to detect spatial variability decreases drastically with depth for irradiance sensors. The detectable variability is dependent on pond size, pond fraction, extinction in the water column, and the light-field geometry represented by  $C$ . We quantified the relative range of variability at a depth  $z$  by

$$\beta^*(z) = \frac{\max(F(z)) - \min(F(z))}{\max(F(z))}. \quad (12)$$

For general comparison, this quantity was scaled with the variability at the sea-ice bottom,

$$\beta(z) = \frac{\beta^*(z)}{\beta^*(z=0)}. \quad (13)$$

Figure 7a shows examples of how the irradiance variability is propagated into the water column for a pond size of 7.5 m and pond fractions of 0.3 and 0.4. While at 20 m depth, 26.9% (10.3%) of the surface variability can be detected assuming  $\gamma = 0$ , up to 47.0% (29.1%) is detectable if  $\gamma = 0.6$  and the pond coverage is 30% (40%). Higher values of  $\gamma$  lead to a deeper propagation of the variability through the water column. It is necessary to assess the variability observable from a certain depth to plan ROV and AUV campaigns. While 90% of the variability can be observed within a distance of 4 m to the ice bottom for all modeled cases with pond sizes bigger than 7.5 m, the spatial variability of ice optical properties can be assessed at depths in excess of 10 m only for ponds larger than 15 m. Large ponds, small pond coverage, and high values of  $\gamma$  generally lead to a better detectability of surface variations at depth. Small ponds, large pond coverage and low values of  $\gamma$  decrease the ability of irradiance sensors to detect surface variability at depth.

## 4. Discussion

### 4.1. Anisotropy of the Light Field

Due to the absence of significant scattering in the underlying water, the radiance distribution underneath sea ice is not isotropic. This is predicted by the theory of radiative transfer [Kokhanovsky and Zege, 2004; van de Hulst, 1980]. Our results clearly confirm that the radiance distribution underneath sea ice is not isotropic. The error introduced by the isotropic assumption is not negligible even if the scattering coefficient of the ice is isotropic ( $\gamma = 0$ ) and can be easily determined using the  $C$  value. When converting radiance to planar irradiance, the assumption of an isotropic radiance field overestimates planar irradiance by a factor  $\pi/C$ . For  $\gamma = 0$ , this is already an overestimation of 25%. For realistic sea-ice cases with  $\gamma = 0.3$  (0.6) planar irradiance is overestimated by 65% (142%). This error is even bigger for scalar irradiance. For  $\gamma = 0$ , scalar irradiance is overestimated by 49%, while the overestimate is 103% (213%) for  $\gamma = 0.3$  (0.6). Thus, the assumption of an isotropic radiance field should not be used to estimate irradiance from radiance. Instead, a  $C$  value  $\leq 2.5$  should be used. Both our modeled  $C = 1.3$  for  $\gamma = 0.6$  as well as our measured  $C = 1.68$  (1.09 ... 1.76) values are similar to the  $C$  value of 1.78 that we reconstructed from the radiance distribution measurements of Trodahl *et al.* [1989].

### 4.2. Influence of an Heterogeneous Sea-Ice Cover

Of importance for the light field beneath sea ice is the influence of structural inhomogeneity on the  $C$  value. Under small areas with high light transmittance, such as melt ponds or cracks in the ice, the radiance distribution is strongly downward-peaked resulting in a lower  $C$  value. Under dark patches such as pressure ridges, more light is received from the sides than from above, increasing the  $C$  value. Thus, the  $C$  value measured from the ratio of irradiance to radiance is only related to the anisotropy parameter of the ice under an ice cover which is sufficiently homogenous or when looking at the median of observations with large spatial extent. This geometric effect is the cause for the scatter in Figure 3, where datapoints with  $C > \pi$  are related to measurements under bright patches

### 4.3. Estimating $C$

Our results show that the  $C$  value has significant implications for the interpretation of under-ice radiation measurements. Nevertheless, it is challenging to estimate  $C$  from the observations of ice properties. The horizontal extinction of light was found to be increasing with bulk salinity [Zhao *et al.*, 2010] which is an indicator of brine volume. Trodahl *et al.* [1989] observed that the anisotropy of the scattering coefficient is dependent on salinity and brine volume, identifying brine channels as the main source of the anisotropy. In our case of melting summer sea ice, brine volume can be approximated by the air volume of the samples as almost all pores are filled with air after sampling. We found a clear dependence of  $\gamma$  on porosity ( $R^2 = 0.956$ ) in our laboratory experiments,

$$\gamma(\Phi) = 2.43 - 0.026 \Phi, \quad (14)$$

indicating that sea ice exhibits a stronger anisotropy of the scattering coefficient with increasing air volume. While the small number of samples did not allow us to investigate the dependence of  $\gamma$  on the columnar texture in depth, we found that the anisotropy tends to increase with the length to width ratio of ice crystals determined by the analysis of vertical thin sections ( $R^2 = 0.29$ ).

In addition to microstructural properties, the  $C$  value is expected to depend on ice optical thickness and on the presence of absorbing material. The radiance distribution under sea ice is affected by absorption from ice algae [Petrich *et al.*, 2012a; Trodahl *et al.*, 1989]. This could explain the low  $C$  value of  $C = 1.09$  at station PS80/360, where high abundances of ice algae in and below the ice were observed with the ROV cameras. Numerical analyses presented are valid for optically thick ice only. In optically thin ice, the transmitted radiance distribution depends on the incident light field. Thus, the presented results cannot be directly applied to estimate the radiance distribution under thin ice (e.g., nilas) and thus differ from the results of Schoonmaker *et al.* [1989] as well as Voss *et al.* [1992].

### 4.4. Multiple Scattering

Trodahl *et al.* [1989] introduced the concept of the anisotropic scattering coefficient in sea ice as a necessity to describe their experimental results. The field measurements of Pegau and Zaneveld [2000] could neither prove nor disprove the concept. In the classical works on scattering in sea ice, small samples of only 1–2

cm<sup>3</sup> were used [Grenfell and Hedrick, 1983; Miller et al., 1997]. A slight dependence of scattering on sample orientation had been found but was considered insignificant. Our samples were significantly bigger, rendering anisotropic extinction more obvious.

We suggest that the anisotropy of the scattering coefficient originates from a nonrandom but ordered distribution of scatterers along brine inclusion planes and scattering at brine channel walls. Thus, the anisotropy should be more pronounced in columnar ice, while the less ordered texture of granular ice should lead to a weak or even no anisotropy of the scattering coefficient. As the spacing of brine inclusion planes and the size of brine channel systems is on the mm to cm scale [Timco and Weeks, 2010], the anisotropy of the scattering coefficient becomes observable only for larger samples when multiple scattering is present. As a result, this anisotropy is not dependent on the phase function of a single scattering event. The systematic configuration of brine inclusions causing anisotropy of the scattering coefficient also causes anisotropy of other physical properties of columnar sea ice such as tensile strength [Timco and Weeks, 2010] and electrical resistivity [Jones et al., 2012].

We conclude from our results that the anisotropic nature of scattering is important for radiative transfer in sea ice and that not all apparent optical properties can be simulated correctly if anisotropy of the scattering coefficient is neglected. In addition, anisotropic light fields have to be taken into account in the simulation of horizontally inhomogeneous ice covers and the angular radiance distribution.

#### 4.5. Brine Drainage

The laboratory measurements have been affected by an almost complete loss of brine. This problem applies to all sea ice sampling in summer, when large brine channels cause an immediate loss of pore water during the extraction of ice cores. We expect our drained samples to show higher scattering and extinction than expected for submerged ice samples because the contrast in refractive index is higher for air in ice than for brine in ice. Nevertheless, we do not expect a significant effect on the measured anisotropy of the scattering coefficient, as the geometry of scattering interfaces like brine channel walls are not influenced by this drainage. While the phase function of single scattering events and the magnitude of the scattering coefficients depend on the refractive index, the anisotropy of the scattering coefficient should be independent of the refractive index as it is determined by the configuration of scatterers.

#### 4.6. Field Measurements of the Radiance Distribution

It is difficult to directly relate laboratory measurements to large-scale ROV measurements as the sea ice texture varies considerably within one ice station. Direct measurements of the angular radiance distribution obtained from rolling the ROV underneath the ice (as shown in Figure 4) can only be interpreted qualitatively, as this is a demanding operation for the ROV pilot due to considerable under-ice currents and thus data quality is low. The measurements are influenced by various factors such as horizontal displacements, rotation of the ROV, inaccurate inclination readings and variations in the not perfectly homogenous ice cover. These and other uncertainties are also discussed in Nicolaus and Katlein [2013]. The determination of  $C$  values from the irradiance to radiance ratio is dependent on the angular sensitivity of the radiance sensor. As a radiance sensor collects light from a finite solid angle, but radiance is mathematically defined for an infinitely small solid angle, the radiance distribution cannot be sampled correctly, when it varies significantly within the field of view of the radiance sensor. For the downward-peaked radiance distributions underneath sea ice this can result in an overestimation of the  $C$  value. This bias can be estimated for a radiance distribution given by equation (10): For  $\gamma = 0.6$ , the radiance distribution varies up to 10% within the sensor footprint of 6°. This can still be regarded as narrow enough, as the absolute calibration uncertainty of the used spectral radiometers is within the order of 5–10% [Nicolaus et al., 2010a].  $C$  values obtained with radiance sensors of a much larger field of view will be significantly skewed toward higher values.

Our simulations were consistent with measurement procedures as radiance distributions were obtained by binning photons exiting the underside of the ice in bins of 5°.

#### 4.7. Scalar Irradiance

Knowledge about the radiance distribution is not only necessary to convert radiance to planar irradiance to determine energy fluxes but also necessary for the conversion of planar irradiance data into scalar irradiance relevant for photosynthesis. For the conversion between planar and scalar irradiance measurements, the influence of anisotropic radiance distributions can be described by the mean cosine  $\bar{\mu}_d$  of the downwelling light field [Maffione and Jaffe, 1995],

$$\bar{\mu}_d = \frac{F}{F_{2\pi}} = \frac{\int_{\phi=0}^{2\pi} \int_{\theta=0}^{\pi/2} L(\theta, \phi) \cos \theta \sin \theta \, d\theta d\phi}{\int_{\phi=0}^{2\pi} \int_{\theta=0}^{\pi/2} L(\theta, \phi) \sin \theta \, d\theta d\phi} \quad (15)$$

From the results of our Monte Carlo simulations, we found for the light field right beneath sea ice  $\bar{\mu}_d=0.59$  and  $\bar{\mu}_d=0.65$  for  $\gamma = 0$  and  $\gamma = 0.6$ , respectively. The dependence of  $\bar{\mu}_d(\gamma)$  is shown in Figure 5b and could be fitted with the polynomial approximation ( $R^2 = 0.998$ )

$$\bar{\mu}_d(\gamma) = 0.5936 + 0.0433 \gamma + 0.0757 \gamma^2. \quad (16)$$

The mean cosine of the downwelling light field in sea ice has not been studied in depth. *Ehn and Mundy* [2013] use  $\bar{\mu}_d=0.7$  based on observations and modeling [*Ehn et al.*, 2008b], while *Arrigo et al.* [1991] used  $\bar{\mu}_d=0.656$ . These numbers agree well with the results of our modeled radiance distributions for sea ice with anisotropic scattering coefficient  $\gamma > 0.6$ .

Combining equations (4) and (16) one can derive the following relation between radiance and spherical irradiance,

$$F_{2\pi} = \frac{F}{\bar{\mu}_d} = \frac{C \cdot L_0}{\bar{\mu}_d}. \quad (17)$$

Both,  $C$  and  $\bar{\mu}_d$  are scalars describing the radiance distribution as a function of the microstructural parameter  $\gamma$ .

#### 4.8. Implications for Field Measurements

The consequences of the downward-peaked radiance distribution on the conversion of radiance measurements to irradiance discussed above are important for future radiation measurements under sea ice. To obtain high-spatial coverage, light measurements will more often be conducted from submersible sensor platforms such as ROVs or AUVs. Due to the collision hazard with under-ice topography, large platforms will have to operate at a certain minimum distance beneath the ice. When using irradiance sensors this distance will lead to a strong areal averaging of light levels and a loss of spatial resolution. However, the spatial variability is important for the small-scale assessment of the energy and mass balance of the ice cover and determination of the light available to ice associated biota for primary production. Hence, missions focusing on the spatial variability of light conditions will need to use radiance sensors to observe the spatial variability of light conditions from depths  $>10$  m. These data can then be transferred into under-ice irradiance readings with conversion methods based on the  $C$  value presented above.

*Frey et al.* [2011] described irradiance maxima under bare ice adjacent to ponds, caused by the large area influencing an irradiance measurement underneath the ice. They reproduced their measurements using a geometric light-field model similar to ours but modeled maximum positions were up to 2 m shallower than the measured position of the irradiance maximum. This discrepancy could be at least partly explained by their assumption of an isotropic light field.

#### 4.9. Future Work

For a better understanding of radiative transfer processes in sea ice and light availability underneath sea ice further investigations of the radiance distribution in and underneath sea ice are necessary. The combination of Monte Carlo models [*Petrich et al.*, 2012a; *Trodahl et al.*, 1987] with three-dimensional measurements of sea-ice microstructure by X-ray microtomographs [*Golden et al.*, 2007; *Kaempfer et al.*, 2007] could reveal more details about microscopic scattering properties. Radiance cameras [*Antoine et al.*, 2012] deployed underneath sea ice would be able to provide a more detailed measurement of the under-ice light field.

### 5. Conclusions

From the synopsis of our field and lab experiments and modeling results, we conclude that the radiance distribution underneath sea ice is not isotropic. In fact the radiance distribution is even more downward directed than predicted by isotropic radiative transfer theory, because scattering in sea ice is anisotropic.

These results show that the commonly used assumption of an isotropic under-ice light-field leads to significant errors in the conversion between radiance and irradiance measurements. We introduced the  $C$  value as a practical measure of light-field geometry. Theoretical and numerical considerations show that  $C \leq 2.5$  should be used rather than  $C = \pi$  in the absence of further information about anisotropic scattering of sea ice, if scattering properties of the sea ice are known and there is no significant contribution of absorption,  $C$  can be estimated from either equations (11) and (14) or microstructural analysis. While one would expect a  $C$  value close to 2.5 for granular ice, smaller values between 1.3 and 2.3 can be assumed for columnar ice. For cold and highly columnar winter-sea ice even lower values could occur. Our geometric light-field model shows that a conversion of radiance to irradiance data will become necessary for light measurements conducted more than 4 m away from the ice underside if the spatial variability is of interest. As a consequence, ROV-based measurements of the variability of under-ice irradiance should be conducted within 4 m distance of the ice underside. To be able to measure the spatial variability of light underneath the sea ice, future AUV and submarine missions will have to use radiance sensors and the suggested conversions in addition to the simultaneous use of irradiance sensors for the quantification of shortwave energy fluxes at depth. Knowledge of the angular radiance distribution also enables for a correct conversion of measurements of planar irradiance to scalar irradiance determining the light available for photosynthetic activity.

### Acknowledgments

We acknowledge the support of the captain, the crew, and the scientific cruise leader Antje Boetius of the RV Polarstern cruise ARK-XXVII/3, facilitating the ROV measurements. Martin Schiller, Larysa Istomina, and Scott Sørensen contributed significantly to the success of the field measurements as part of the group. We thank two anonymous reviewers for their constructive comments improving the manuscript. This study was funded through the Alfred-Wegener-Institut Helmholtz-Zentrum für Polar- und Meeresforschung. C.P. acknowledges support of the Research Council of Norway, project 195153 (ColdTech).

### References

- Antoine, D., et al. (2012), Underwater radiance distributions measured with miniaturized multispectral radiance cameras, *J. Atmos. Oceanic Technol.*, 30(1), 74–95, doi:10.1175/JTECH-D-11-00215.1.
- Arrigo, K. R., C. W. Sullivan, and J. N. Kremer (1991), A biooptical model of Antarctic sea ice, *J. Geophys. Res.*, 96(C6), 10,581–10,592, doi:10.1029/91JC00455.
- Bélangier, S., S. A. Cizmeli, J. Ehn, A. Matsuoka, D. Doxaran, S. Hooker, and M. Babin (2013), Light absorption and partitioning in Arctic Ocean surface waters: Impact of multiyear ice melting, *Biogeosciences*, 10(10), 6433–6452, doi:10.5194/bg-10-6433-2013.
- Cox, G. F. N., and W. F. Weeks (1983), Equations for determining the gas and brine volumes in sea-ice samples, *J. Glaciol.*, 29(102), 306–316.
- Ehn, J. K., and C. J. Mundy (2013), Assessment of light absorption within highly scattering bottom sea ice from under-ice light measurements: Implications for Arctic ice algae primary production, *Limnol. Oceanogr. Methods*, 58(3), 893–902, doi:10.4319/lo.2013.58.3.0893.
- Ehn, J. K., C. J. Mundy, and D. G. Barber (2008a), Bio-optical and structural properties inferred from irradiance measurements within the bottommost layers in an Arctic landfast sea ice cover, *J. Geophys. Res.*, 113, C03503, doi:10.1029/2007JC004194.
- Ehn, J. K., T. N. Papakyriakou, and D. G. Barber (2008b), Inference of optical properties from radiation profiles within melting landfast sea ice, *J. Geophys. Res.*, 113, C09024, doi:10.1029/2007JC004656.
- Ehn, J. K., C. J. Mundy, D. G. Barber, H. Hop, A. Rossnagel, and J. Stewart (2011), Impact of horizontal spreading on light propagation in melt pond covered seasonal sea ice in the Canadian Arctic, *J. Geophys. Res.*, 116, C00G02, doi:10.1029/2010JC006908.
- Eicken, H., H. R. Krouse, D. Kadko, and D. K. Perovich (2002), Tracer studies of pathways and rates of meltwater transport through Arctic summer sea ice, *J. Geophys. Res.*, 107(C10), 8046, doi:10.1029/2000JC000583.
- Frey, K. E., D. K. Perovich, and B. Light (2011), The spatial distribution of solar radiation under a melting Arctic sea ice cover, *Geophys. Res. Lett.*, 38, L22501, doi:10.1029/2011GL049421.
- Golden, K. M., H. Eicken, A. L. Heaton, J. Miner, D. J. Pringle, and J. Zhu (2007), Thermal evolution of permeability and microstructure in sea ice, *Geophys. Res. Lett.*, 34, L16501, doi:10.1029/2007GL030447.
- Grenfell, T. C. (1977), The optical properties of ice and snow in the arctic basin, *J. Glaciol.*, 18(80), 445–463.
- Grenfell, T. C., and D. Hedrick (1983), Scattering of visible and near infrared radiation by NaCl ice and glacier ice, *Cold Reg. Sci. Technol.*, 8(2), 119–127, doi:10.1016/0165-232x(83)90003-4.
- Grenfell, T. C., and D. K. Perovich (1981), Radiation absorption coefficients of polycrystalline ice from 400–1400 nm, *J. Geophys. Res.*, 86(NC8), 7447–7450, doi:10.1029/JC086iC08p07447.
- Haas, C., A. Pfaffling, S. Hendricks, L. Rabenstein, J.-L. Etienne, and I. Rigor (2008), Reduced ice thickness in Arctic Transpolar Drift favors rapid ice retreat, *Geophys. Res. Lett.*, 35, L17501, doi:10.1029/2008GL034457.
- Haines, E. M., R. G. Buckley, and H. J. Trodahl (1997), Determination of the depth dependent scattering coefficient in sea ice, *J. Geophys. Res.*, 102(C1), 1141–1151, doi:10.1029/96JC02861.
- Hamre, B., J. G. Winther, S. Gerland, J. J. Starnes, and K. Starnes (2004), Modeled and measured optical transmittance of snow-covered first-year sea ice in Kongsfjorden, Svalbard, *J. Geophys. Res.*, 109, C10006, doi:10.1029/2003JC001926.
- Jaffé, A. (1960), Über Strahlungseigenschaften des Gletschereises, *Arch. Meteorol. Geophys. Biokl. B.*, 10(3), 376–395, doi:10.1007/BF02243201.
- Jones, K. A., M. Ingham, and H. Eicken (2012), Modeling the anisotropic brine microstructure in first-year Arctic sea ice, *J. Geophys. Res.*, 117, C02005, doi:10.1029/2011JC007607.
- Kaempfer, T. U., M. A. Hopkins, and D. K. Perovich (2007), A three-dimensional microstructure-based photon-tracking model of radiative transfer in snow, *J. Geophys. Res.*, 112, D24113, doi:10.1029/2006JD008239.
- Kokhanovsky, A. A., and E. P. Zege (2004), Scattering optics of snow, *Appl. Opt.*, 43(7), 1589–1602, doi:10.1364/AO.43.001589.
- Krembs, C., H. Eicken, and J. W. Deming (2011), Exopolymer alteration of physical properties of sea ice and implications for ice habitability and biogeochemistry in a warmer Arctic, *Proc. Natl. Acad. Sci. U. S. A.*, 108(9), 3653–3658, doi:10.1073/pnas.1100701108.
- Leu, E., J. Wiktor, J. E. Soreide, J. Berge, and S. Falk-Petersen (2010), Increased irradiance reduces food quality of sea ice algae, *Mar. Ecol. Prog. Ser.*, 411, 49–60, doi:10.3354/meps08647.
- Light, B., G. A. Maykut, and T. C. Grenfell (2003), A two-dimensional Monte Carlo model of radiative transfer in sea ice, *J. Geophys. Res.*, 108(C7), 3219, doi:10.1029/2002JC001513.
- Light, B., T. C. Grenfell, and D. K. Perovich (2008), Transmission and absorption of solar radiation by Arctic sea ice during the melt season, *J. Geophys. Res.*, 113, C03023, doi:10.1029/2006JC003977.



- Maffione, R. A., and J. S. Jaffe (1995), The average cosine due to an isotropic light source in the ocean, *J. Geophys. Res.*, *100*(C7), 13,179–13,192, doi:10.1029/95JC00461.
- Maffione, R. A., J. M. Voss, and C. D. Mobley (1998), Theory and measurements of the complete beam spread function of sea ice, *Limnol. Oceanogr.*, *43*(1), 34–43, doi:10.4319/lo.1998.43.1.0034.
- Maslanik, J. A., C. Fowler, J. Stroeve, S. Drobot, J. Zwally, D. Yi, and W. Emery (2007), A younger, thinner Arctic ice cover: Increased potential for rapid, extensive sea-ice loss, *Geophys. Res. Lett.*, *34*, L24501, doi:10.1029/2007GL032043.
- Miller, D., M. S. QuinbyHunt, and A. J. Hunt (1997), Laboratory studies of angle- and polarization-dependent light scattering in sea ice, *Appl. Opt.*, *36*(6), 1278–1288, doi:10.1364/ao.36.001278.
- Mobley, C. D., G. F. Cota, T. C. Grenfell, R. A. Maffione, W. S. Pegau, and D. K. Perovich (1998), Modeling light propagation in sea ice, *IEEE Trans. Geosci. Remote Sens.*, *36*(5), 1743–1749, doi:10.1109/36.718642.
- Mundy, C. J., D. G. Barber, and C. Michel (2005), Variability of snow and ice thermal, physical and optical properties pertinent to sea ice algae biomass during spring, *J. Mar. Syst.*, *58*(3–4), 107–120, doi:10.1016/j.jmarsys.2005.07.003.
- Nicolaus, M., and C. Katlein (2013), Mapping radiation transfer through sea ice using a remotely operated vehicle (ROV), *Cryosphere*, *7*(3), 763–777, doi:10.5194/tc-7-763-2013.
- Nicolaus, M., S. R. Hudson, S. Gerland, and K. Munderloh (2010a), A modern concept for autonomous and continuous measurements of spectral albedo and transmittance of sea ice, *Cold Reg. Sci. Technol.*, *62*(1), 14–28, doi:10.1016/j.coldregions.2010.03.001.
- Nicolaus, M., S. Gerland, S. R. Hudson, S. Hanson, J. Haapala, and D. K. Perovich (2010b), Seasonality of spectral albedo and transmittance as observed in the Arctic Transpolar Drift in 2007, *J. Geophys. Res.*, *115*, C11011, doi:10.1029/2009JC006074.
- Nicolaus, M., C. Katlein, J. Maslanik, and S. Hendricks (2012), Changes in Arctic sea ice result in increasing light transmittance and absorption, *Geophys. Res. Lett.*, *39*, L24501, doi:10.1029/2012GL053738.
- Pegau, W. S., and J. R. V. Zaneveld (2000), Field measurements of in-ice radiance, *Cold Reg. Sci. Technol.*, *31*(1), 33–46, doi:10.1016/s0165-232x(00)00004-5.
- Perovich, D. K. (1990), Theoretical estimates of light reflection and transmission by spatially complex and temporally varying sea ice covers, *J. Geophys. Res.*, *95*(C6), 9557–9567, doi:10.1029/JC095iC06p09557.
- Perovich, D. K. (2011), The changing Arctic sea ice cover, *Oceanography*, *24*(3), 162–173.
- Perovich, D. K., K. F. Jones, B. Light, H. Eicken, T. Markus, J. Stroeve, and R. Lindsay (2011), Solar partitioning in a changing Arctic sea-ice cover, *Ann. Glaciol.*, *52*(57), 192–196.
- Petrich, C., M. Nicolaus, and R. Gradinger (2012a), Sensitivity of the light field under sea ice to spatially inhomogeneous optical properties and incident light assessed with three-dimensional Monte Carlo radiative transfer simulations, *Cold Reg. Sci. Technol.*, *73*, 1–11, doi:10.1016/j.coldregions.2011.12.004.
- Petrich, C., H. Eicken, J. Zhang, J. Krieger, Y. Fukamachi, and K. I. Ohshima (2012b), Coastal landfast sea ice decay and breakup in northern Alaska: Key processes and seasonal prediction, *J. Geophys. Res.*, *117*, C02003, doi:10.1029/2011JC007339.
- Roesel, A., and L. Kaleschke (2012), Exceptional melt pond occurrence in the years 2007 and 2011 on the Arctic sea ice revealed from MODIS satellite data, *J. Geophys. Res.*, *117*, C05018, doi:10.1029/2011JC007869.
- Roulet, R. R., G. A. Maykut, and I. C. Grenfell (1974), Spectrophotometers for the measurement of light in polar ice and snow, *Appl. Opt.*, *13*(7), 1652–1659, doi:10.1364/ao.13.001652.
- Schoonmaker, J. S., K. J. Voss, and G. D. Gilbert (1989), Laboratory measurements of optical beams in young sea ice, *Limnol. Oceanogr.*, *34*(8), 1606–1613.
- Serreze, M. C., M. M. Holland, and J. Stroeve (2007), Perspectives on the Arctic's shrinking sea-ice cover, *Science*, *315*(5818), 1533–1536, doi:10.1126/science.1139426.
- Timco, G. W., and W. F. Weeks (2010), A review of the engineering properties of sea ice, *Cold Reg. Sci. Technol.*, *60*(2), 107–129, doi:10.1016/j.coldregions.2009.10.003.
- Trodahl, H. J., R. G. Buckley, and S. Brown (1987), Diffusive transport of light in sea ice, *Appl. Opt.*, *26*(15), 3005–3011, doi:10.1364/AO.26.003005.
- Trodahl, H. J., R. G. Buckley, and M. Vignaux (1989), Anisotropic light radiance in and under sea ice, *Cold Reg. Sci. Technol.*, *16*(3), 305–308, doi:10.1016/0165-232x(89)90030-x.
- van de Hulst, H. C. (1980), *Multiple Light Scattering: Tables, Formulas, and Applications*, Academic, New York.
- Voss, J. M., R. C. Honey, G. D. Gilbert, and R. R. Buntzen (1992), Measuring the point-spread function of sea ice in situ, in *Proceedings of the SPIE Ocean Optics XI*, 1750, doi:10.1117/12.140682.
- Zeebe, R. E., H. Eicken, D. H. Robinson, D. WolfGladrow, and G. S. Dieckmann (1996), Modeling the heating and melting of sea ice through light absorption by microalgae, *J. Geophys. Res.*, *101*(C1), 1163–1181, doi:10.1029/95JC02687.
- Zhao, J. P., T. Li, D. Barber, J. P. Ren, M. Pucko, S. J. Li, and X. Li (2010), Attenuation of lateral propagating light in sea ice measured with an artificial lamp in winter Arctic, *Cold Reg. Sci. Technol.*, *61*(1), 6–12, doi:10.1016/j.coldregions.2009.12.006.